JOURNAL OF MOLECULAR SPECTROSCOPY 56, 167–187 (1975)

Rotational Analysis of the 5933 Å Band of NO_2[1]

CHARLES G. STEVENS[2] AND RICHARD N. ZARE

Department of Chemistry, Columbia University, New York, New York 10027

By exciting NO_2 with a narrow band (0.035 cm^{-1} FWHM) tunable dye laser in the region of 5935 Å, an extensive analysis of the $K = 0, 1$, and 2 subbands of a vibronic transition has been carried out. The analysis of this transition proves that the upper state has the electronic symmetry $^2B_2$. The origin of the analyzed band is placed at 16 849.48 cm^{-1} and the following molecular constants provide a best fit to the measured line positions: $A_v = 7.85$ cm^{-1}, $B_v = 0.451$ cm^{-1}, $C_v = 0.394$ cm^{-1}, and $\epsilon_{bb} + \epsilon_{cc} = -0.0877$ cm^{-1}. The band exhibits a number of obvious perturbations with a marked intensity falloff for increasing N and K values. Large centrifugal distortion constants are required, apparently caused by N-dependent perturbations. A large inertial defect, $\Delta = 3.26$ amu Å^2, is also found. By attributing the inertial defect to the vibrational dependence of A_v, we estimate the geometry for the NO_2 $^2B_2$ excited state extrapolated to the vibrational origin to be $r_0 = 1.31$ Å and $\theta_0 = 111°$.

I. INTRODUCTION

The visible absorption spectrum of NO_2 (shown in Fig. 1) has long been a source of frustration to spectroscopists because of its complex vibrational and rotational structure which has proved highly resistant to analysis by traditional methods. At least two electronic transitions, $^2B_2 \leftarrow {}^2A_1$ and $^2B_1 \leftarrow {}^2A_1$, are predicted by theoretical studies (*1*) to provide the major absorption strength in this visible region, with smaller contributions expected from the forbidden $^2A_2 \leftarrow {}^2A_1$ as well as possible quartet–doublet transitions. Another source of complexity is anticipated in the spectrum of NO_2 through the possible interaction of the low-lying electronic states caused by the breakdown of the Born–Oppenheimer (BO) approximation.

In the parlance of radiationless transitions, the low-lying electronic states of NO_2 represent a prime example of "intermediate case" states (*2*) in which a given BO state interacts with a relatively sparse set of neighboring states. It is this sparseness of interacting levels which can give rise, in large part, to the complexity of the spectrum since the distribution of interacting states is not a smooth function of energy, as found, for example, in large molecules or in predissociation. Indirect evidence that the upper states in this system of NO_2 are indeed perturbed has been provided by numerous lifetime studies (*3*) that have yielded lifetimes which are longer by more than one order of magnitude than estimates based on integrated absorption coefficient measurements. This so-called anomolous lifetime behavior is predicted to be characteristic of "intermediate case" states undergoing radiationless processes (*4*).

[1] This work was supported by grant NSF-GP-31336 from the National Science Foundation.

[2] Present address: Lawrence Livermore Laboratory, Mail Station L-211, University of California, Livermore, California 94550.

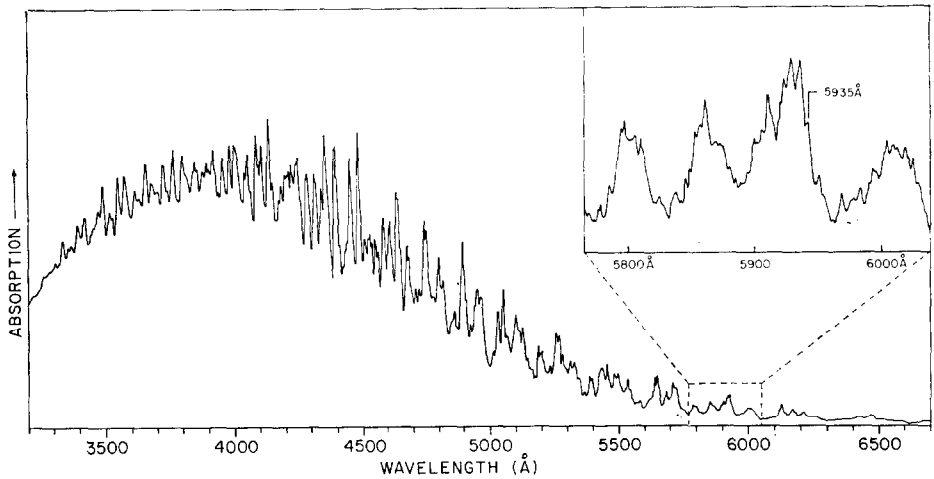

FIG. 1. Low-resolution absorption spectrum of NO_2. The inset shows an expanded region under higher resolution. The shoulder at 5935 Å marks the region which has been extensively investigated using laser-induced fluorescence. The spectra were kindly made available to us by R. Pirkle and J. C. D. Brand (University of Western Ontario).

Traditional spectroscopic methods have met with some success in analyzing a number of relatively unperturbed K = 0 subbands of the $^2B_1 \leftarrow {}^2A_1$ transition (*5*). The identification and analysis of transitions to the $^2B_2$ state has represented more of a challenge. Success has, in the main, relied upon the development of new experimental techniques. Using the technique of laser-induced fluorescence, Abe and co-workers (*6*) and also Brand *et al.* (*7*) have succeeded in exciting several rotational levels of the $^2B_2 \leftarrow {}^2A_1$ transition within the narrow bandwidth of their fixed frequency lasers. These studies have yielded partial information about the rotational structure of the $^2B_2$ state. The newly developed technique of microwave optical double resonance (MODR), with microwave transitions occurring both in the excited state (*8*) and ground state (*9*) has a sub-Doppler width resolution and opens a new dimension to experimental investigations of complex systems. In particular, MODR in the ground state permits the assignment of the fine and hyperfine components of the optical transition, while MODR in the excited state permits the location of nearby levels not optically connected to the ground state. Another technique which circumvents the Doppler-width limitations to high-resolution spectroscopy has been demonstrated by Demtröder, Paech, and Schmiedl using a molecular beam of NO_2 excited at right angles with a single-mode argon ion laser (*10*). By tuning the laser through the 5145 Å line, hyperfine transitions of NO_2 have been observed. Quite recently, Bird and Marsden (*11*) have reported the observation of pure rotational resonance Raman scattering from NO_2 using several ion laser lines. Rotational analysis of the scattered light has enabled them to identify the vibronic symmetry from which they have been able to deduce the presence of the $^2B_2$ and $^2B_1$ electronic states at the laser frequencies employed.

Laser-induced fluorescence using tunable lasers offers the flexibility in excitation frequency necessary to provide a systematic and complete examination of the rotational transitions of a vibrational band. This technique was first applied to the visible system of NO_2 (*12*) and several rotational assignments made of a $K = 0$ subband asso-

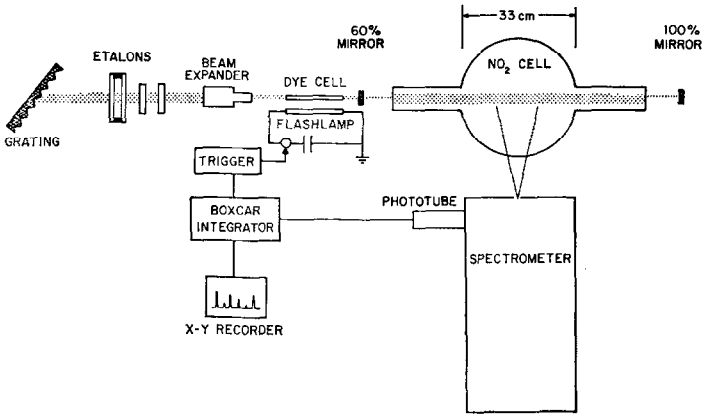

FIG. 2. Block diagram of experimental apparatus.

ciated with the $^2B_2 \leftarrow {}^2A_1$ transition in the region near 5935 Å (see inset in Fig. 1). We report now the results of an extensive examination of the $K = 0$, 1, and 2 subbands of this system. This provides a verification of the $^2B_2$ electronic nature of the upper state as well as estimates of the equilibrium structure of the upper state.

II. EXPERIMENTAL DETAILS

A. Fluorescence Excitation and Detection

The experimental apparatus used for the laser-induced fluorescence studies (see Fig. 2) is a somewhat modified version of that reported previously (*12*). The active medium of the dye laser is a rhodamine 6G/methanol solution which circulates through a quartz tube located along one focal line of a polished aluminum elliptical cavity (MgF_2 overcoated). A commercial xenon flashlamp (Xenon Corp.) lies along the other focal line, surrounded by a quartz water jacket. Both the quartz tube and the flashlamp have the dimensions 13 cm × 0.3 cm. It is found necessary to maintain the average temperature of the circulating water between 15°C and 25°C. Lower temperatures resulted in the deposition of a yellowish material on the lamp wall near the center while higher temperatures resulted in the deposition of a bronze-colored material. A discharge of typically 11 joules/pulse of electrical energy (0.1 μF at 15 KV) is passed through the lamp by triggering a hydrogen thyratron (EG & G model 1802) at a pulse rate of 5–7 pps. The concentration of the dye is adjusted to give maximum output at the wavelength region of interest. The pulse width of the laser energy is approximately 200 nsec FWHM.

The laser cavity is terminated at one end by a 60% reflecting mirror and at the other by an 1800 line/mm grating (PTR optics) operated in first order. The laser bandwidth is narrowed using a 6X beam expander and several etalons. The principal etalon (Coherent Radiation model 760) consists of two air-spaced quartz plates whose outer surfaces are wedged to avoid interference effects. The inner surfaces have a reflectivity of approximately 30% at 5935 Å. The plate separation was adjusted to give a free spectral range (FSR) of 4.37 cm^{-1}, which exceeds the bandpass of the grating ($\sim$3 cm^{-1} full width). This etalon decreases the laser bandwidth from approximately 1 cm^{-1} to 0.25 cm^{-1} FWHM. At a fixed grating angle, the laser can be tuned approximately 1.5 cm^{-1}

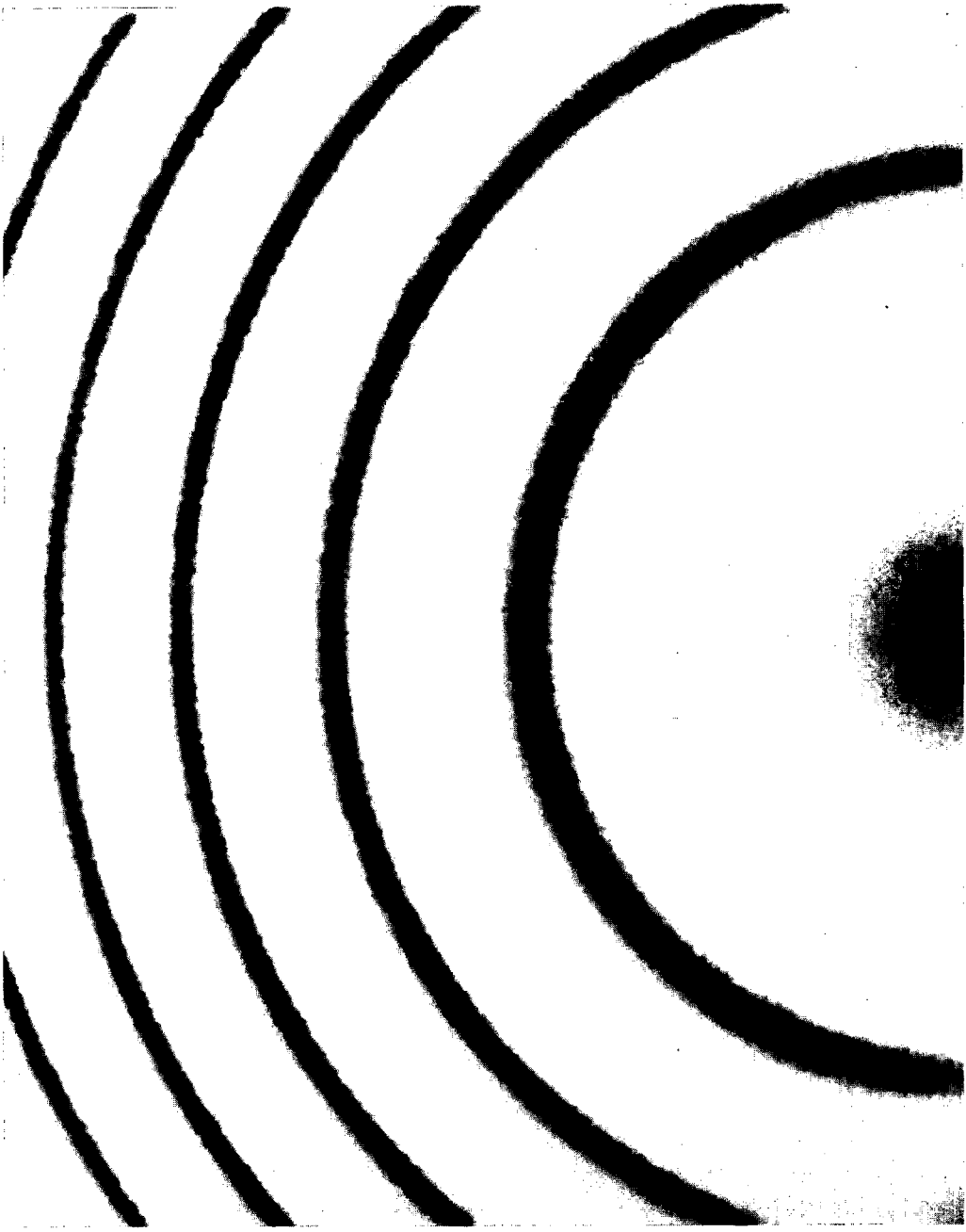

about the center frequency passed by the grating without jumping to an adjacent order of the etalon. The etalon is situated in a thermally lagged housing and maintained at a constant temperature (±0.05°C) by circulating water from a constant-temperature bath through the brass housing. Further narrowing of the laser bandwidth is achieved by the use of two quartz plates (uncoated, $\lambda/20$ flatness) which serve as auxiliary etalons. The plate thicknesses are 1 cm (FSR $\sim$ 0.34 cm^{-1}) and 0.3 cm (FSR $\sim$ 1.14 cm^{-1}) and decrease the laser bandwidth to 0.035 cm^{-1} FWHM, as determined interferometrically (see Fig. 3). The auxiliary etalons increase the average intensity/cm^{-1} somewhat and dramatically improve the frequency stability.

The fluorescence cell is placed inside an external multiple-reflection cavity formed by refocusing the laser beam back into the dye cavity by means of a 100% reflecting mirror (3 m radius of curvature). The fluorescence signal increases by a factor greater than 4 over single-pass intensity.

The fluorescence is collected by a lens and observed at right angles to the excitation direction with a 1 m spectrometer (SPEX 1704) equipped with curved slits and a 1200 line/mm grating blazed for maximum efficiency at 10 000 Å. Emission spectra are recorded in second order which provides a dispersion of $\sim$3.2 Å/mm. A dove prism is used to rotate the fluorescence image into coincidence with the spectrometer slit orientation. The signal from an EMI 9659 photomultiplier (S-20 response) is fed into a PAR CW-1 boxcar integrator using a 15 μsec observation window initiated by the laser trigger. The fluorescence spectra are obtained by scanning the spectrometer with a stepping motor (typically at 0.9 Å/min for high-resolution spectra) through the spectral region of interest. For rotationally resolved studies, the absolute wavelength of the NO_2 lines is established by simultaneously recording the known standard lines of a Ne emission lamp. In this way, the measurement accuracy of the NO_2 fluorescence lines is ±0.1 Å.

B. NO_2 Samples

The NO_2 (Matheson, 99.5% pure) is stored in a liquid nitrogen-cooled coldfinger. To obtain an NO_2 sample, the coldfinger is raised in temperature using a dry-ice–acetone bath and the condensate is pumped on to remove the more volatile constituents. After several freezing–pumping cycles the NO_2 is admitted to the fluorescence cell. Only NO_2 from pure white condensate is used. This purification procedure proved not to be critical except for lifetime studies. The pressure for the fluorescence studies was in the range of 20–50 mTorr, as determined by a thermocouple gauge (calibration checked against the known vapor pressure of NO_2 at the temperature of the dry-ice–acetone bath). The gas handling system is grease-free as well as mercury-free.

C. Absorption Spectrum

The high-resolution absorption spectrum was photographed by M. M. Hessel using a Kodak 103 emulsion in second order on the Argonne National Laboratory (*13*) 9.1 m concave-grating spectrograph with a dispersion of about 0.36 Å/mm. Frequencies were measured relative to thorium emission line standards (*13*, *14*) using a Grant photoelectric comparator. The reproducibility for unblended lines was approximately ±0.01 cm^{-1}.

FIG. 3. Interference fringes photographically recorded (200 laser shots). The separationbe tween the fringescorresponds to 0.727 cm^{-1} and the measured FWHM is 0.035 cm^{-1}.

D. Laser Frequency Tuning

With the help of the 1 m spectrometer, the grating and primary etalon are tuned simultaneously to the frequency of a standard Ne emission line located in the vicinity of a desired excitation frequency. The fine tuning of the laser frequency so that it comes into coincidence with an absorption line is accomplished as follows. The etalon is fastened to an optical mount equipped with precision vernier micrometers. The micrometers are scaled to 10^{-4} inch and rotate the etalon about the vertical axis with a 3 inch lever arm. The laser frequency as a function of etalon rotation can be established by using the resonance condition

$$\nu\ (\mathrm{cm}^{-1}) = m/2nh \cos\theta, \tag{1}$$

where θ is the angle with respect to normal incidence to the inner reflective surfaces, h is the plate separation (in cm), n the refractive index of the etalon medium (air in this case), and m is the order passed by the etalon. For small angles of rotation, $\cos\theta$ can be replaced by $(1 + \frac{1}{2}d^2/b^2)^{-1}$, where b is the lever arm length and d is the micrometer head displacement from normal incidence (normal incidence causes laser action to occur off the etalon reflective surfaces, allowing a convenient means of establishing this orientation). The dependence of laser frequency on the micrometer head position is established from Eq. (1) by considering two frequencies in the same order m. The change in laser frequency from ν_1 to $\nu_2 = \nu_1 + \Delta\nu$ in the same order m resulting from a change in micrometer position from d_1 to $d_2 = d_1 + \Delta d$ is given by

$$\Delta\nu/\Delta d = [(d_1 + d_2)/2](\nu_1/b^2). \tag{2}$$

Thus, provided $d^2 \ll b^2$, the change in frequency ($\Delta\nu$) resulting from a change in micrometer setting (Δd) is proportional to the mean displacement from normal incidence. Given a known frequency (ν_1) at one displacement (d_1) and a desired frequency (ν_2), the new micrometer setting (d_2) is given then by rearranging expression (2) to yield

$$d_2 = [d_1^2 + (\nu_2/\nu_1 - 1)2b^2]^{\frac{1}{2}}. \tag{3}$$

This expression is independent of the nature of the etalon (free spectral range, etc.) and requires only knowledge of the length of the rotation lever arm. This length can be established empirically by tuning the laser from coincidence with one Ne standard line frequency to another. In this way, the tuning calibration was established and provided a tuning precision of better than 5%. That is, tuning the laser 2 cm^{-1} places the frequency within 0.1 cm^{-1} of the desired value. Knowledge of the free spectral range of the etalon then enables tuning of the laser to any desired frequency with this precision. Fine tuning of the laser onto an absorption line is then accomplished by maximizing fluorescence intensity.

III. RESULTS

Figure 4 shows a low-resolution fluorescence spectrum, uncorrected for photomultiplier and spectrometer response, resulting from excitation at 5935.6 Å. The relative fluorescence intensities are characteristic of the emission caused by excitation in the region 5930–5940 Å indicating that the strongly absorbing states in this region all have similar vibrational character (Franck–Condon factors). Furthermore, the strength of the absorption and fluorescence together with results of the rotational analysis argue that the transition is electronically allowed. The strong fluorescence derives from excitation of the totally symmetric ground vibrational level. For an electronically allowed transition, the prominent fluorescence features correspond to transitions between states

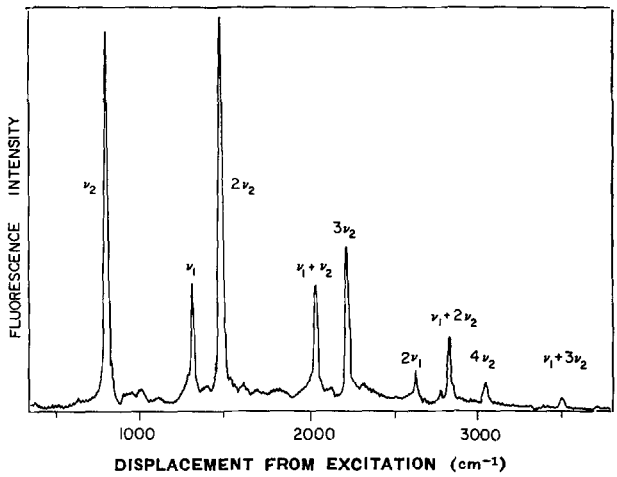

FIG. 4. Low-resolution (~20 cm^{-1}) fluorescence spectrum for excitation at 5935.6 Å at 50 mTorr NO_2 pressure.

of the same vibrational symmetry. Thus we conclude from the absence of emission to odd quanta of ν_3 (symmetry b_2) that the upper-state vibrational symmetry is totally symmetric.

Much weaker vibronic transitions are also observed at various wavelengths in this region. A "hot" band originating from the (0, 1, 0) vibrational level of the ground state is excited here and gives rise to a weak (<0.1% of the strong emission) transition, detected in the anti-Stokes region. In addition, weak features are observed, as reported previously (*12*), which are best interpreted as originating from a $^2B_1$ upper state.

Transitions to these states as well as transitions involving the tails of nearby vibronic states and perturbation-derived energy levels give rise to an apparent absorption continuum in this region at Doppler-limited resolution. The intensity of this background absorption continuum contributes as much as 20% of the intensity of the strongest resolved lines, as determined from the absorption spectrum and from the unresolved laser excitation spectrum. The continuum is most pronounced where the resolved NO_2 lines appear in the absorption spectrum, and seem to disappear where there are no NO_2 vibronic transitions.

Rotationally resolved fluorescence spectra were obtained by monitoring the emission to the $3\nu_2$ level of the ground state. Emission to this band is less intense than to either ν_2 or $2\nu_2$ (see Fig. 4) but allows a considerably better determination of the value of the quantum number K involved in the transition. This arises because of the large interaction in the NO_2 ground state between rotation about the top axis (a-axis) and the bending vibrational mode (ν_2), which causes the rotational constant A to have the vibrational dependence, $A_v = A_0 - \alpha_2^0 v_2 - \gamma_2^0 v_2^2$. Considering only progressions in ν_2 and transitions between levels having the same N, K values, the displacement from the excitation energy of a fluorescence line for a near-symmetric rotor can be approximated by the expression (*15*)

$$\Delta E(v_2) = E(0, v_2, 0; N, K) - E(0, 0, 0; N, K) = \omega_2^0 v_2 + x_{22}^0 v_2^2 + (\bar{B}_{v_2} - \bar{B}_0)N(N+1) + [(A_{v_2} - A_0) + (\bar{B}_{v_2} - \bar{B}_0)]K^2. \quad (4)$$

Since in the ground state of NO_2, $\bar{B}_{v_2} \cong \bar{B}_0$ the expression reduces to

$$\Delta E(v_2) = \omega_2{}^0 v_2 + x_{22}{}^0 v_2{}^2 - (\alpha_2{}^0 v_2 + \gamma_2{}^0 v_2{}^2)K^2. \tag{5}$$

Using recently determined values for the constants (*16*) gives the energy difference (cm^{-1}) $\Delta E(3) = 2246.07 + 1.16K^2$ and the significant dependence of ΔE on K is apparent.

Figure 5 shows rotationally resolved fluorescence spectra which illustrate this K dependence. Excitation energies were used where several transitions lie within the laser bandwidth. The expected origins for the transition sequence $N \rightarrow N'$ in absorption followed by $N' \rightarrow N$ in emission for $K = 0, 1$, and 2 are indicated by arrows in the figure. The identification of the K value is unambiguous at the resolution employed (~ 1 cm^{-1} FWHM). The displacements, $\Delta E(3)$, determined from the fluorescence spectra are 2246.0 ± 0.2, 2247.2 ± 0.2, and 2250.8 ± 0.2 cm^{-1} for $K = 0$, 1, and 2 respectively, in good agreement with the values calculated using Eq. (5).

The emission line pattern is characteristic of a parallel (a-axis) transition following $\Delta K = 0$ selection rules. In general, only P- and R-emission lines are observed with the present excitation intensity, the Q lines being considerably weaker, as expected for a parallel transition (*15*). The identification of an absorption line as a P- or R-branch member follows simply from the appearance of transitions to either the low-energy side (P) or the high energy side (R) of the K origin line, as shown in Fig. 5. The identification of the N values involved is made by comparing the fluorescence line separation with known ground state energy differences. The ground state energies were calculated using a complete matrix diagonalization doublet–asymmetric rotor computer program developed in J. C. D. Brand's laboratory.[3] The ground state rotational constants reported by Hurlock *et al.* (*16*) were used along with the microwave-determined spin constants (*17*).

A densitometer tracing of the high-resolution absorption spectrum in this region is shown in Figs. 6–8. The P, Q, and R branches in $K = 0$, 1, and 2 are clearly separated and consequently the transitions are simply labeled by the upper-state quantum number N' (K is the same in both states). Those transitions that have been identified by fluorescence analysis are indicated by solid lines; the dashed lines identify transitions that have been assigned by ground state combination differences. Individual Q-branch members are not labeled.

Examination of the N' values in $K = 0$ shows that even members of the branch are missing. This arises as a consequence of the nuclear spin statistics in $N^{16}O_2$ which allow only levels of A_1 or A_2 spinrovibronic symmetry to exist [In Hund's case (b) states, the spin functions are totally symmetric (*18*).] Only a $^2B_2$ state has missing even N values for $K = 0$, thus providing direct proof of the vibronic symmetry of the upper state.[4] As mentioned earlier, the absence of odd quanta of ν_3 in the fluorescence spectrum requires the upper state to have only totally symmetric vibrational symmetry. This establishes the $^2B_2$ electronic symmetry for this state.

[3] We thank J. C. D. Brand and J. L. Hardwick (University of Western Ontario) as well as C. Seliskar (University of Cincinnati) for making programs available to us.

[4] The use of C_{2v} symmetry is not meant to imply that the NO bond lengths are necessarily equal, since tunneling through a reasonably small barrier allows the molecule to exhibit the same nuclear spin statistics.

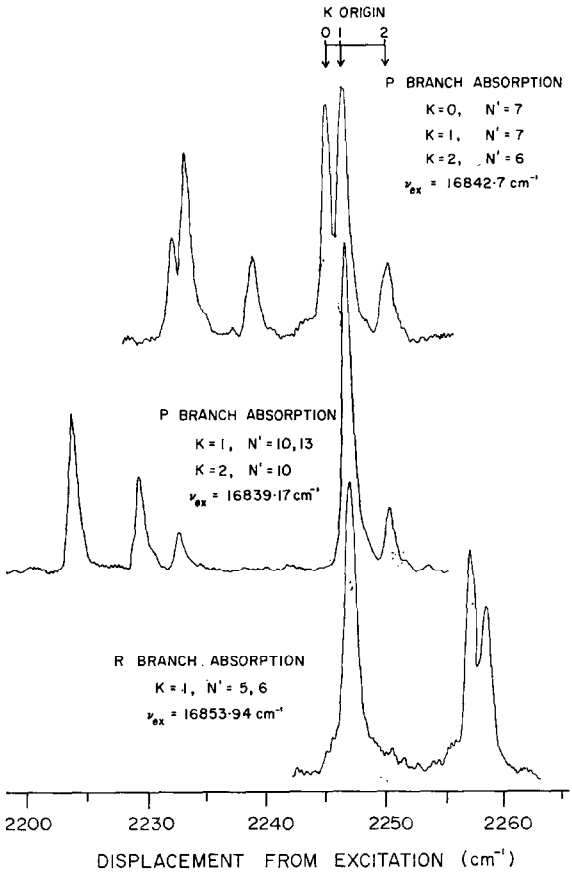

FIG. 5. High-resolution ($\sim$1 cm^{-1}) fluorescence spectra in the region of $3\nu_2$ for excitation in the 5933 Å band at 50 mTorr NO_2 pressure.

A large number of the transitions are found as doublets with the same upper-state N value. These are indicated in Figs. 6–8 by the doubled lines. Anticipating the results of the analysis, these doublets are ascribed to transitions involving the two spin components $F_1(J = N + \frac{1}{2})$ and $F_2(J = N - \frac{1}{2})$.

In Table I we present a listing of the line positions (in cm^{-1}) and their assignments. All P-branch members shown have been identified from their fluorescence spectrum. The R-branch members are assigned on the basis of ground state combination differences. In some cases (indicated by asterisks) the assignments have been verified by fluorescence. The last column of Table I gives the difference between the observed R-branch member position and the position calculated by adding ground state energy differences to the observed position of the corresponding P-branch member. In assigning the R-branch transitions, the presence of spin doubling in the ground state sometimes gives rise to ambiguities. If the spin splitting in the ground state is sufficiently large, i.e., larger than the uncertainty due to line position measurement or blending, a unique assignment of a transition as either $F_1 \rightarrow F_1$ or $F_2 \rightarrow F_2$ can be made. This appears to be the case in the $K = 1$, $N' = 2$ and 3 transitions and the choice made is shown in the

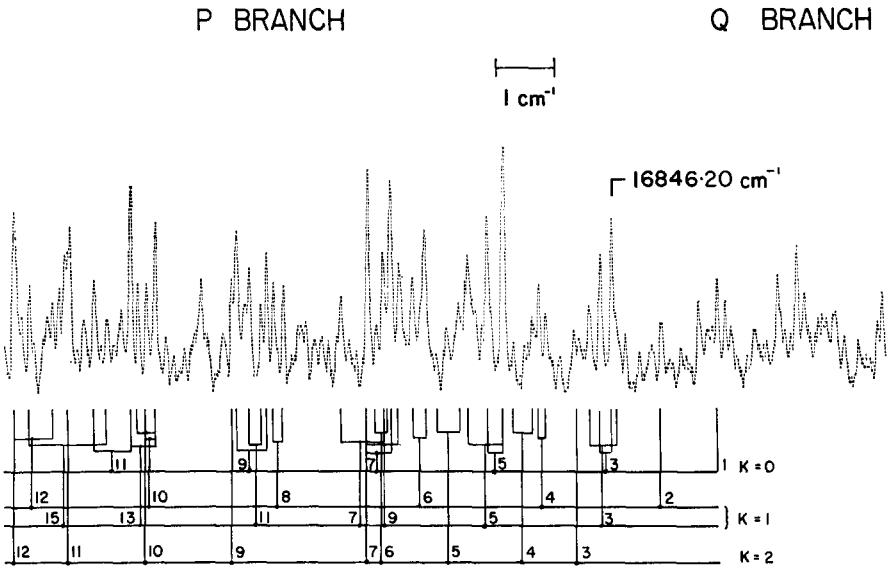

FIG. 6. Densitometer tracing of high-resolution absorption spectrum (P branch, low N' values) with assignments.

last column of Table I. If the spin splitting is comparable to the line position uncertainty, then we are confronted with a choice which is indicated in Table I. If only one entry is listed for the line position of the R-branch member, then either choice of spin components leads to a unique line assignment, i.e., a choice of either F_1 or F_2 for the P-branch member leads to only one possible line assignment for the corresponding R-branch member. Dual entries in this column occur in the lower N' values of $K = 2$ where the two choices lead to two different (adjacent) lines for the corresponding

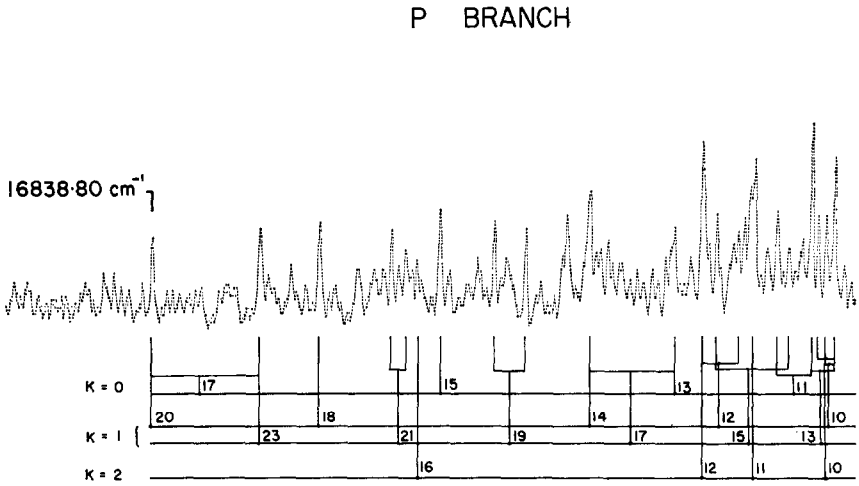

FIG. 7. Densitometer tracing of high-resolution absorption spectrum (P branch, high N' values) with assignments.

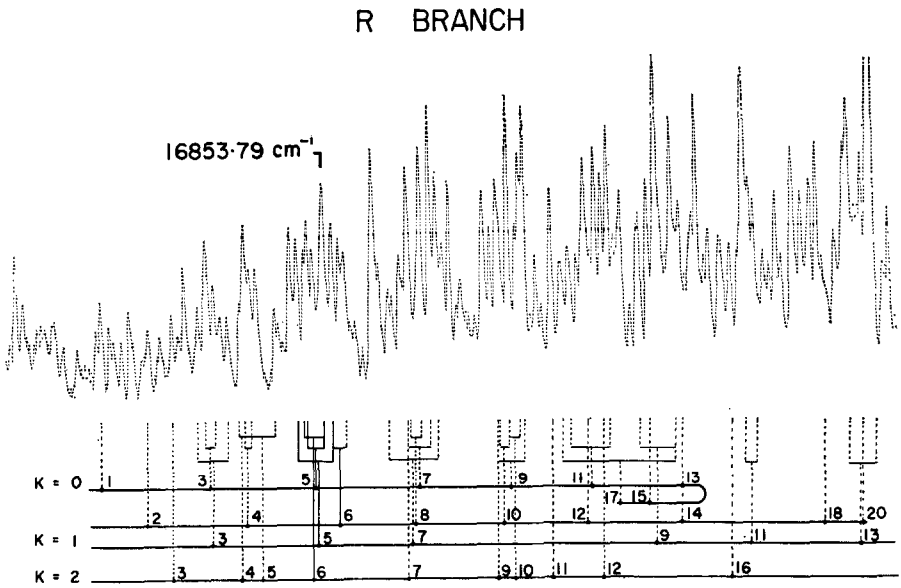

FIG. 8. Densitometer tracing of high-resolution absorption spectrum (R branch) with assignments.

R-branch member. The low absorption intensity of these transitions prevents reliance upon the quality of the residuals in making the assignment. Dual entries in the last column are made where the two choices lead to differences exceeding 0.01 cm^{-1}. We have also marked in Table I those transitions identified by microwave-optical double-resonance studies of Tanaka *et al.* (*9*).

The quality of the fit of the R-branch members by combination differences is reasonably good. The discrepancies between observed and calculated values, which are somewhat larger than the uncertainty in line position measurements, are apparently caused by the blending of lines. In particular the large discrepancy (0.05 cm^{-1}) for $K = 0$, $N' = 3$ at 16 851.99 cm^{-1} arises from a blend with an unidentified stronger feature.

The intensity distribution in this band (see Figs. 6–8) is decidedly non-Boltzmann. The peak intensity at room temperature in the P branch should occur at $N' = 15$. In $K = 0$, however, the branch peaks at $N' = 7$ and rapidly diminishes in intensity with the last observed member being $N' = 17$. There are no prominent absorption lines belonging to this band at longer wavelengths. A similar intensity falloff is seen for $K = 1$ and $K = 2$. The P-branch transition to $N' = 7, K = 0$ gives rise to the strongest emission intensity with a sharp drop in intensity at $N' = 9$, $K = 0$. The system also loses intensity prematurely as a function of K, both in absorption and in emission. The intensity ratios of the $K = 1$ to the $K = 0$ subband and the $K = 2$ to the $K = 0$ subband should be approximately 0.9 and 0.67, whereas the observed ratios are roughly 0.5 and 0.2, respectively.

In the R-branch region of the spectrum, there are a number of strong absorption features which appear to be caused by a band whose origin lies further to the blue. Laser-induced fluorescence has been obtained for the relatively intense unassigned fea-

TABLE I

ROTATIONAL ASSIGNMENTS FOR 16 848 cm^{-1} BAND OF THE NO_2 $^2B_2 \leftarrow {}^2A_1$ TRANSITION

P-Branch members[a]			*R*-Branch members[b]			
$N_{K_{-1},K_{+1}}'$	$N_{K_{-1},K_{+1}}''$	ν (cm^{-1})	$N_{K_{-1},K_{+1}}''$	ν (cm^{-1})	obs–calc (cm^{-1}) F_1	F_2
1_{01}	2_{02}	16 847.82[c]	0_{00}	16 850.37[c]	0.00	
3_{03}	4_{04}	46.20[c]	2_{02}	52.11[c]	0.00	
		46.03[c]		51.99[c]	0.05	
5_{05}	6_{06}	44.52[c]	4_{04}	53.79[c]	−0.01*	
		44.28[c]		53.55[c]	−0.01*	
7_{07}	8_{08}	42.79[c]	6_{06}	55.44[c]	0.00	
		42.44[c]		55.11[c]	0.02	
9_{09}	$10_{0,10}$	40.88[c]	8_{08}	56.89[c]	−0.01	
		40.41[c]		56.46[c]	0.03	
$11_{0,11}$	$12_{0,12}$	38.80[c]	$10_{0,10}$	58.20[c]	0.01	
		38.23[c]		57.59[c]	−0.03	
$13_{0,13}$	$14_{0,14}$	36.56	$12_{0,12}$	59.30[c]	0.00	
$15_{0,15}$	$16_{0,16}$	32.72[c]	$14_{0,14}$	58.81[c]	0.00	
$17_{0,17}$	$18_{0,18}$	27.76	$16_{0,16}$	57.18	−0.02	
		27.99		57.45	−0.02	
2_{12}	3_{13}	46.96[c]	1_{11}	51.09	−0.01	
3_{12}	4_{13}	46.27	2_{11}	52.31		0.03
		45.86[c]		51.86[c]	0.01	
4_{14}	5_{15}	45.18[c]	3_{13}	52.66[c]	0.00	−0.02
		45.08[c]		52.58[c]	0.03	0.00
5_{14}	6_{15}	44.52	4_{13}	53.94	0.00*	
		43.98		53.39	0.01	
6_{16}	7_{17}	43.31[c]	5_{15}	54.12[c]	0.007	−0.02
		43.13[c]		53.94[c]	0.005	−0.02*
7_{16}	8_{17}	42.68	6_{15}	55.53	0.02	
		42.03		54.84	−0.02	
8_{18}	9_{19}	41.13[c]	7_{17}	55.28[c]		−0.01
		40.98[c]		55.11[c]	0.00	
9_{18}	10_{19}	42.93	8_{17}	59.18	0.00	
		42.44		58.68	−0.01	
$10_{1,10}$	$11_{1,11}$	39.17[c]	9_{19}	56.66[c]	0.01	
		39.04		56.50	0.01	
$11_{1,10}$	$12_{1,11}$	40.79	10_{19}	60.44	−0.02	
		40.60		60.29	−0.02	
$12_{1,12}$	$13_{1,13}$	37.60	$11_{1,11}$	58.38	0.02	
		37.01[c]		57.81	0.00	
$13_{1,12}$	$14_{1,13}$	39.17	$12_{1,11}$	62.26	0.02	
		38.80		61.91	−0.00	
$14_{1,14}$	$15_{1,15}$	35.16[c]	$13_{1,13}$	59.30[c]	0.01	
$15_{1,14}$	$16_{1,15}$	37.25	$14_{1,13}$	63.74	−0.01	
$17_{1,16}$	$18_{1,17}$	36.56	$16_{1,15}$	66.61	0.06	
		35.11		69.99	−0.02	
$18_{1,18}$	$19_{1,19}$	30.74	$17_{1,17}$	61.52	0.01	
$19_{1,18}$	$20_{1,19}$	34.13	$18_{1,17}$	67.42	−0.02	
		33.61		66.94	0.01	

TABLE I—(*continued*)

P-Branch members[a]			*R*-Branch members[b]			
$N_{K_{-1},K_{+1}}'$	$N_{K_{-1},K_{+1}}''$	ν (cm^{-1})	$N_{K_{-1},K_{+1}}''$	ν (cm^{-1})	obs–calc (cm^{-1})	
					F_1	F_2
$20_{1,20}$	$21_{1,21}$	27.99	$19_{1,19}$	62.11	0.03	
$21_{1,20}$	$22_{1,21}$	32.15	$20_{1,19}$	68.92	0.05	
		31.92		68.64	0.00	
$23_{1,22}$	$24_{1,23}$	29.76	$22_{1,21}$	69.91	0.04	
3_{21}	4_{22}	45.62[c]	2_{20}	51.46, 51.66	0.02	0.04
4_{23}	5_{24}	44.99[c]	3_{22}	52.58, 52.66[c]	0.03	−0.03
		44.67		52.19, 52.31	−0.04	0.00
5_{23}	6_{24}	43.85	4_{22}	53.17	0.05	−0.00
		43.31		52.58, 53.66	−0.00	0.02
6_{25}	7_{26}	42.79	5_{24}	53.74, 53.78	−0.02	0.00*
		42.57		53.51, 53.55	0.00	−0.02*
7_{25}	8_{26}	42.44	6_{24}	55.11	0.00	−0.01
9_{27}	10_{28}	40.36	8_{26}	56.46	0.05	0.03
10_{29}	$11_{2,10}$	39.17	9_{28}	56.88	0.00	0.02
		38.91		56.64	0.01	0.00
11_{29}	$12_{2,10}$	37.84	10_{28}	57.31	0.02	0.01
$12_{2,11}$	$13_{2,12}$	37.01	$11_{2,10}$	58.10	0.00	−0.01
$16_{2,15}$	$17_{2,16}$	32.34	$12_{2,10}$	60.21	0.04	0.03

[a] Identified by laser-induced fluorescence.
[b] Assigned by ground state combination differences. Asterisks denotes verification by fluorescence.
[c] Also observed and assigned by Tanaka and Harris (*23*).

ture lying between the $R(4)$ and $R(6)$ branch members of $K = 0$ (see Fig. 8). This has been identified as a P-branch transition with $N' = 15, K = 3$. The location of the $K = 3$ P branch at this energy (16 854.56 cm^{-1}) is not expected, based on the location of the $K = 1$ and $K = 2$ subbands.

IV. ANALYSIS

A. Rotational Line Fit

A full asymmetric rotor matrix diagonalization computer program for doublet states was used to analyze the spectra. The program is based upon the asymmetric rotor formulations of Raynes (*19*) and includes matrix elements due to spin interactions of the types $\langle NK\,|H|\,NK\rangle$, $\langle NK\,|H|\,N\,K \pm 2\rangle$, $\langle NK\,|H|\,N-1\,K\rangle$, and $\langle NK\,|H|\,N-1\,K \pm 2\rangle$. The program adjusts the rotational and spin constants in an iterative manner to obtain a least-squares fit to the observed line positions. The upper-state constants are free to vary while the ground state constants are fixed to rotational constants from infrared studies (*16*) and the spin constants from microwave studies (*17*). The calculated line positions for this band revealed the presence of numerous perturbations. As a consequence, the significance of including high-order terms in the analysis, such as the spin matrix elements off-diagonal in both N and K, are difficult to assess.

TABLE II

OBSERVED AND CALCULATED[a] K=0 LINE POSITIONS FOR P BRANCH MEMBERS

TRANSITION $N'_{K_{-1},K_{+1}}$	$N''_{K_{-1},K_{+1}}$	ASSIGNED SPIN COMPONENT	ν_{OBS} (cm^{-1})	ν_{CALC} (cm^{-1})	$\nu_{OBS-CALC}$ (cm^{-1})
1_{01}	2_{02}	F_1	16847·74[b]	16847·77	-0·03
		F_2	47·82	47·84	-0·02
3_{03}	4_{04}	F_1	46·03	46·04	-0·01
		F_2	46·20	46·19	0·01
5_{05}	6_{06}	F_1	44·28	44·27	0·01
		F_2	44·52	44·51	0·01
7_{07}	8_{08}	F_1	42·44	42·43	0·01
		F_2	42·79	42·77	0·02
9_{09}	$10_{0\,10}$	F_1	40·41	40·44	-0·03
		F_2	40·88	40·89	-0·01
$11_{0\,11}$	$12_{0\,12}$	F_1	38·24	38·22	0·02
		F_2	38·80	38·80	0·00
$13_{0\,13}$	$14_{0\,14}$	F_1		35·67	
		F_2	36·56	36·39	0·17
$15_{0\,15}$	$16_{0\,16}$	F_1	32·72	32·67	0·05
		F_2		33·55	
$17_{0\,17}$	$18_{0\,18}$	F_1	28·00	29·09	-1·09
		F_2	29·76	30·15	-0·39

[a] Line positions are calculated using both ground and upper state spin matrix elements.

[b] This line, seen in the absorption spectrum, has been assigned on the basis of providing the best fit; its fluorescence spectrum was not investigated.

In the $K = 0$ subband, the analysis including spin effects provides a quite satisfactory fit to the observed line positions up through $N' = 11$, as shown in Table II. The assignments of the $F_1 \leftrightarrow F_1$ and $F_2 \leftrightarrow F_2$ transitions is based upon two points: (1) the sign of the spin constant $(\epsilon_{bb} + \epsilon_{cc})/2$ is determined by the relative positions of F_1 and F_2 in $N' = 9$, $K = 0$ as determined by the microwave study of Tanaka *et al.* (*9*); and (2) the ability of the present assignment to reproduce the remainder of the $K = 0$ line positions. For $N' = 13$ and 15 we have located only one spin component, and at $N' = 17$ both spin components are seen but the fit has clearly gone awry.

The $K = 1$ and $K = 2$ subbands appear to be substantially more perturbed than the $K = 0$ subband, and it is not possible to assign the spin components unambiguously, except for the low N' values of $K = 1$ (see Table I). Instead, the $K = 1$ subband was fit by comparing the mean of the two observed line positions for a fixed N' value with the two possible calculated line positions. Where only one spin component was observed, it was omitted from the fit.

In carrying out the fitting procedure, only N' values up through 11 were used for $K = 0$, and the N' values of 2–6, 8, and 10–13 were used for $K = 1$. No N' values for $K = 2$ were used in the analysis since the constants obtained from $K = 0$ and $K = 1$ provided a satisfactory fit for $K = 2$. Moreover, inclusion of $K = 2$ in the analysis did not seem warranted because of the larger scatter associated with this weaker and somewhat more perturbed subband.

Table III lists the upper-state molecular constants derived from this analysis, and Fig. 9 illustrates the quality of the fit obtained for all the observed P-branch members.

TABLE III

DERIVED UPPER STATE MOLECULAR CONSTANTS FOR THE NO_2 $^2B_2$ 5933 Å BAND

MOLECULAR CONSTANT	VALUE (cm^{-1})
T_v	16849·48
A_v	7·85
$\bar{B}_v$	0·4224
B_v	0·451
C_v	0·394
$\epsilon_{bb} + \epsilon_{cc}$	-0·0877
D_N (K=0,2)	$3·5 \times 10^{-5}$
D_N (K=1)	4×10^{-6}

We have plotted in Fig. 9 the difference between the observed and calculated line positions as a function of the excited state quantum number N'. For the $K = 0$ subband the residuals are formed by comparing the observed line positions with those calculated using the full Hamiltonian including spin interaction. For $N' \leq 11$, the residuals for the F_1 and F_2 spin components coincide with the accuracy of the figure. For the $K = 1$ and $K = 2$ subbands, the residuals represent the difference between the observed line positions and the mean of the calculated $F_1 \leftrightarrow F_1$ and $F_2 \leftrightarrow F_2$ transitions.

We have chosen to display separately in Fig. 9 the $K = 1$ subband residuals for even N' and odd N'. A sharp perturbation in the odd N' values of the $K = 1$ subband is readily apparent, and dashed lines have been included in Fig. 9 to serve as an aid in recognizing the trends in the residuals. The fit found for the members of the $K = 0$ subband and the $K = 1$ subband (even N' values) is quite satisfactory for the lower N' values. In $K = 2$ there is a larger scatter present in Fig. 9 but it appears to be randomly distributed about the mean of the calculated position, which is based on the constants determined from $K = 0$ and $K = 1$. The general appearance of the spin splittings in the $K = 1$ subband allows qualitative estimates to be made regarding the magnitudes and signs of the spin–rotation constants. To a first approximation,[5] the spin splittings in the $K = 1$ subband can be represented, using Lin's notation (*20*), as

$$(F_1 - F_2)/(N + \tfrac{1}{2}) = \bar{\epsilon}_{bb} + (\epsilon_{aa} - \bar{\epsilon}_{bb})/N(N + 1) \pm (\epsilon_{cc} - \epsilon_{bb})/4, \qquad (6)$$

where $\bar{\epsilon}_{bb} = \frac{1}{2}(\epsilon_{bb} + \epsilon_{cc})$, F_1 and F_2 are the energies, and the (+) and (−) signs are associated with the even N' and odd N' values, respectively, for the $^2B_2$ state considered here. The absence of any observable trend that could be attributed to the $(\epsilon_{aa} - \epsilon_{bb})/N(N + 1)$ term argues in Eq. (6) that $|\epsilon_{aa}|$ is less than a few tenths of a cm^{-1}. The much larger splittings associated with odd N' values coupled with the negative sign of

[5] It should be noted that these conclusions are based upon the assumption that the observed splittings are not caused by interactions with local states and that the effective spin–rotation Hamiltonian derived from a Van Vleck transformation retains its validity. The well-behaved nature of the $K = 0$ spin splittings would seem to justify the assumption in this subband.

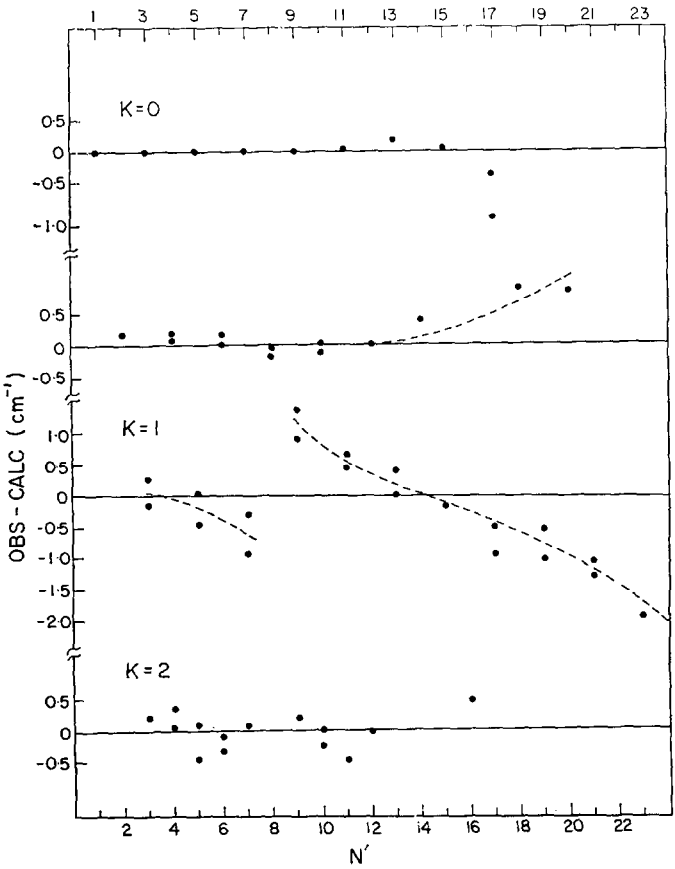

FIG. 9. Deviations between the observed and calculated line positions as a function of the excited state rotational quantum number N'.

$\bar{\epsilon}_{bb}$ determined from $K = 0$ suggests that ϵ_{bb} is negative and larger than ϵ_{cc}. Using the mean splittings for the even and odd N' values in the region $3 \leq N' \leq 13$ and setting $(\epsilon_{aa} - \bar{\epsilon}_{bb})/N(N+1) = 0$ yields a rough value for ϵ_{bb} of approximately -0.08 cm^{-1}, while ϵ_{cc} is determined to be less than 0.01 cm^{-1}.

Note that in Table III the centrifugal distortion constant D_N is unusually large and a separate value is required for $K = 1$ different from $K = 0$ and $K = 2$. The magnitude of the D_N values and the fact that it differs for $K = 0$, $K = 2$, and $K = 1$, together with the dramatic intensity falloff as N' or K increases, argue for the presence of a substantial interaction between this state and a number of others.

B. Perturbations

In addition to the smooth N'- and K-dependent perturbations, there is a sharp perturbation seen in the $K = 1$ subband (see Fig. 9). This sharp perturbation is interesting in that a distinction is made on the basis of even and odd N' values. A strong interaction is seen in both the F_1 and F_2 components of the odd N' levels cutting between $N' = 7$ and $N' = 9$ with a maximum resonance at $N' = 9$, whereas little or no interaction is observed in the even N' levels in this region. The observation that the perturbation

affects both the F_1 and F_2 components requires that the perturbing levels have the same N value (selection rule $\Delta N = 0$) in order to conserve J. A microwave-optical double-resonance signal from the 9_{09} level of this system to a level, called x, lying 47.6 GHz higher in energy has been observed by Tanaka, Field, and Harris (*21*). They have concluded that this mystery transition is to a $J = 19/2$ rotational state of some other vibronic state which perturbs the $^2B_2$, 9_{18} level. Using the known energies, this x level lies approximately 8.65 cm^{-1} below the directly observed 9_{18} ($J = 19/2$) level (assuming the lower energy transition is assigned $F_1 \leftarrow F_2$). The displacement of this level from its unperturbed position is approximately 1.2 cm^{-1}. For a two-state interaction scheme in which the perturbing states are displaced equally in energy, the unperturbed position of the x level would be placed approximately 6.25 cm^{-1} below the unperturbed position of the 9_{18} level and an interaction matrix element of approximately 3 cm^{-1} would account for the observations. However, it does not seem possible, on the basis of a simple two-state model, to place a perturbing level 6.25 cm^{-1} below the 9_{18} state and also above the 7_{16} level (with $\Delta N = 0$) without making unreasonable demands on the $\bar{B}$ value of the perturbing state. Since the unperturbed separation of the 9_{18} and 7_{16} levels is approximately 17.7 cm^{-1}, the separation of the corresponding $N = 9$ and $N = 7$ levels of the perturbing state would at best (assuming an N-dependent matrix element) be roughly 6 cm^{-1} requiring a $\bar{B}$ value of 0.18 cm^{-1}. Furthermore, the displacements involving $N' = 5$ and 11 would not be reproduced. The possibility that more than one vibronic state is responsible seems unlikely in view of the regular behavior of the displacements. A further possibility is that a single state is responsible but due to simultaneous interactions between the two principal states and others, the resulting energy displacements are unsymmetrical.

The distinction made between even and odd N' values can occur with $\Delta K = 0$ selection rules by allowing the $K = 1$ energy levels of the perturbing state to correspond closely to a symmetric top. The asymmetry distortion of the observed $^2B_2$, $K = 1$ energy levels would then allow one set (odd N') to come into resonance with the perturbing state while affecting only a subtle displacement of the even N' energy levels. Similarly, the $K = 2$ energy levels of a perturbing state could give rise to this distinction. An appealing candidate for interaction is the $K = 0$ sublevels of a perturbing state when, due to nuclear spin statistics, only one set (even or odd) of N' levels exists, and an obvious distinction is made. The condition that $\Delta N = 0$ requires this state to be a vibronic $^2B_1$ state providing interaction with the odd N' values only. The electronic $^2B_1$ state can couple with the $^2B_2$ state through the interaction electronic orbital motion about the b-axis (symmetry z-axis) with either molecular rotation or electronic spin (spin–orbit) about this axis providing $\Delta K = \pm 1$ selection rules. If, indeed, the $^2B_1$ electronic state is responsible for the perturbation, an estimate of the frequency of the symmetric stretching motion of this state is possible. Using the origin of the $^2B_1$ state determined by Brand and Hardwicke (*5*) and assuming a $\bar{B}$ value of 0.37 cm^{-1} (in qualitative agreement with the observed perturbation) would place the origin of this $^2B_1$ vibrational state at 16 862 cm^{-1}. The (0, 1, 0) band origin is calculated to be at $\sim$15 662 cm^{-1}, which leaves a difference of 1200 cm^{-1} as the vibrational frequency of the symmetric stretching mode of this state. If the above interpretation is correct, then progressions in upper-state ν_2 differing by $\sim$1200 cm^{-1} from the fundamental progression should be observable in absorption.

Speculation regarding the nature of the perturbing state(s) is a particularly tenuous endeavor without substantial experimental information to provide guidelines. The uncertainties are compounded in multiplet states where spin–orbit coupling must be entertained along with the possibilities of vibration–rotation (Coriolis), vibration–electronic, and rotation–electronic coupling between states as well as higher-order combinations of these interactions.

Verification of a particular mechanism should be possible using laser-induced fluorescence since the rotational fluorescence of the mixed state will, in most cases, differ from the pure state. Examination of the rotational structure of the emission from the perturbed 9_{18} level failed, however, to provide information regarding the nature of the perturbing state. Several weak emission lines are observed which do not correspond to the expected P and R transitions from 9_{18} but the low intensity of these features has prevented a detailed interpretation. More intense laser excitation should allow a definitive investigation of the nature of these interactions.

V. DISCUSSION

The technique of tunable, narrow-band laser-induced fluorescence has proved to be an incisive probe of the rotational structure of this band. The results have revealed the presence of numerous perturbations in this band which make assignments by traditional techniques exceedingly difficult and fraught with uncertainties. We have succeeded in assigning approximately 130 transitions in the NO_2 5933 Å band and we find that the upper-state energy levels are well represented, on the whole, by the formulas appropriate to a near-prolate symmetric top ($\kappa_v = -0.994$). Although we do not now understand the nature of the observed anomalous intensity distribution, the present analysis enables us to determine the geometry of the excited state. Of course such a determination is subject to the possible uncertainties arising from a failure to completely deperturb the system. Nevertheless, we believe it is possible to extract a meaningful albeit approximate structure of the NO_2 $^2B_2$ excited state from the moments of inertia obtained in this analysis.

The NO_2 molecule is a 17-valence–electron system. A qualitative picture of the geometry expected for the electronic states of NO_2 is provided by the Walsh diagrams (*22*). The NO_2 $X\ ^2A_1$ ground state has the electronic configuration $(1a_1)^2\ (1b_2)^2\ (2a_1)^2\ (1b_1)^2\ (3a_1)^2\ (2b_2)^2\ (3b_2)^2\ (1a_2)^2\ (4a_1)$ and is predicted to be bent, where we use the notation and ordering of the molecular orbitals given by Burnelle *et al.* (*1a*). The lowest-lying NO_2 $^2B_2$ state has the electronic configuration $(1a_1)^2\ (1b_2)^2\ (2a_1)^2\ (1b_1)^2\ (3a_1)^2\ (2b_2)^2\ (3b_2)\ (1a_2)^2\ (4a_1)^2$ and is also predicted to be bent. The 90° conformation is heavily favored by the $(4a_1)$ orbital while the $(3b_2)$ orbital shows a slight preference for the 180° conformation. Since the NO_2 $^2B_2$ state differs from the $X\ ^2A_1$ state by the promotion of an electron from the bonding $(3b_2)$ orbital to the nonbonding $(4a_1)$ orbital, the Walsh diagram predicts that (1) the $^2B_2$ state of NO_2 should have a substantially more acute bond angle than the ground state, and (2) the NO bond distance in the $^2B_2$ state should be longer than in the $X\ ^2A_1$ state.

We turn now to the determination of the excited state geometry from the deduced molecular constants. The values of the rotational constants given in Table III for $K = 0$, 1, and 2 ought to be regarded as phenomenological in that they simply represent constants which reproduce the residuals reported. The D_N constant used in the analysis

must obviously be viewed in this sense because of the different value required for $K = 1$ and also because of the significant intensity decrease with increasing N. Furthermore, the observation of $N' = 15$, $K = 3$ at 16 854.56 cm^{-1} questions the mechanical significance of the A_v value reported here. We have been informed (*23*) that a number of observations of P-branch members of $K = 3$ and $K = 4$ subbands have been located to the blue of the 16 849.48 cm^{-1} band origin. Assuming that these higher K subbands are associated with the same upper-vibronic state, their location requires an A_v value considerably larger than the 7.85 cm^{-1} found for $K = 1$ and 2. A perturbing state coming into resonance between $K = 2$ and $K = 3$ would account for this observation. An alternative explanation is that the apparent band system in this region is a composite of vibronic states derived from a given Born–Oppenheimer state interacting with a number of other states. The resulting spectrum is then derived from transitions to these daughter states having, on the whole, complementary intensity distributions, i.e., the sum of the individual intensity distributions would recapture the Boltzmann distribution for a near-symmetric top. It is felt that the constants B and C represent more nearly the constants of mechanical significance for this band. In particular, the interactions responsible for the large apparent distortion correction have a strong dependence on the quantum number N and plots of the residuals, not including this correction, smoothly approach zero residual values in an asymptotic fashion as one approaches low values of N. Hence, the fit to low values of N excluding distortion extrapolates to essentially the same B and C values as those obtained using higher N values including distortion. The $\bar{B}$ value reported here differs somewhat from that reported by Abe (*6a*) in the 5145 Å region (0.477 cm^{-1}) and by Brand (*7*) in the 6470 Å region (0.345 cm^{-1}). However, as pointed out by these authors, the possibility that the constants obtained are determined in part by local perturbations (*7*) or different vibronic transitions (*6a*) cannot be ruled out in view of the limited number of rotational levels excited.

The large inertial defect found for this band, $\Delta = 3.26$ amu Å^2, can be attributed to nonrigid rotation about any or all of the three major axes. In the ground state of NO_2, the interaction of the bending vibration and rotation about the a-axis gives rise to a substantial dependence of the A_v value on the number of vibrational quanta excited; on the other hand, the B_v and C_v constants show little dependence on the bending motion. Brand and co-workers (*7*) have tentatively made the vibrational assignment of the 5933 Å band as $1_0^1\, 2_0^5\, 3_0^0$. Thus, given the fact that the A_v value is already suspect in view of the possible perturbation of the K sublevels, together with the expected strong dependence of A_v on the number of bending quanta excited, we make the assumption that the inertial defect is contained wholely in A_v. With the further assumption that B_v and C_v do not depend on the vibrational state, a rough estimate of the N–O bond length and the O–N–O bond angle at the (0, 0, 0) origin of the $^2B_2$ state is made of $r_0 = 1.31$ Å and $\theta_0 = 111°$. Although our estimates of r_0 and θ_0 are admittedly quite crude, we cannot doubt their qualitative significance, namely, that the NO_2 $^2B_2$ state is considerably more bent than the NO_2 $^2A_1$ ground state (*24*) ($\theta_0 = 134.25°$) and that the bond length of the $^2B_2$ state is significantly longer than that of the $^2A_1$ ground state ($r_0 = 1.197$ Å). These findings are in agreement with the qualitative arguments based on the simple Walsh diagrams. The values obtained here may be compared to the theoretically calculated equilibrium values of Burnell, May, and Gangi (*1a*) who find $\theta_e = 101.3°$ and with the most recent ab initio calculations of Gillespie *et al.* (*25*) who

find $\theta_e = 101.7°$, and $r_e = 1.26$ Å. The qualitative discrepancy between the extrapolated experimental geometry determined here and the best calculated geometry is presumably caused primarily by our failure either to fully deperturb the analyzed band or to accurately account for the vibrational dependence of the rotational constants. The analysis of additional bands by laser-induced fluorescence will provide increased confidence in the geometry of the NO_2 $^2B_2$ excited state and further our understanding of the nature of the interactions responsible for the perturbations seen in this system.

ACKNOWLEDGMENTS

We thank John Brand, John Hardwick, and Carl Seliskar for making computer programs available to us; Takehiko Tanaka and David Harris for making information available to us prior to publication; Merrill Hessel for providing us with the high-resolution plates of NO_2; and Rod Wallace for contributions toward the improvement of the optical quality of the flashlamp-pumped dye laser.

RECEIVED: October 21, 1974

REFERENCES

1. (a) L. BURNELLE, A. M. MAY, AND R. A. GANGI, *J. Chem. Phys.* **49**, 561 (1968); R. A. GANGI AND L. BURNELLE, *J. Chem. Phys.* **55**, 843, 851 (1971). (b) W. H. FINK, *J. Chem. Phys.* **49**, 5054 (1968); **54**, 2911 (1971). (c) J. E. DELBENE, *J. Chem. Phys.* **54**, 3487 (1971). (d) P. J. HAY, *J. Chem. Phys.* **58**, 4706 (1973).
2. G. W. ROBINSON AND R. P. FROSCH, *J. Chem. Phys.* **38**, 1187 (1963); G. W. ROBINSON, *J. Chem. Phys.* **47**, 1967 (1967); K. F. FREED AND J. JORTNER, *J. Chem. Phys.* **50**, 2916 (1969); M. BIXON AND J. JORTNER, *J. Chem. Phys.* **50**, 3284 (1969).
3. D. NEUBERGER AND A. B. F. DUNCAN, *J. Chem. Phys.* **22**, 1693 (1954); K. SAKURAI AND H. P. BROIDA, *J. Chem. Phys.* **50**, 2404 (1969); K. SAKURAI AND G. CAPELLE, *J. Chem. Phys.* **53**, 3764 (1970); L. F. KEYSER, F. KAUFMAN, AND E. C. ZIPF, *Chem. Phys. Lett.* **2**, 523 (1968); L. F. KEYSER, S. Z. LEVINE, AND F. KAUFMAN, *J. Chem. Phys.* **54**, 355 (1971); S. E. SCHWARTZ AND H. S. JOHNSTON, *J. Chem. Phys.* **51**, 1286 (1969); P. R. LEBRETON, W. MECKLENBRAUCK, A. SCHULTZ, AND C. SCHLIER, *J. Chem. Phys.* **55**, 2940 (1971); P. B. SACKETT AND J. T. YARDLEY, *Chem. Phys. Lett.* **6**, 323 (1970); *J. Chem. Phys.* **57**, 152 (1972).
4. A. E. DOUGLAS, *J. Chem. Phys.* **45**, 1007 (1966).
5. A. E. DOUGLAS AND K. P. HUBER, *Can. J. Phys.* **43**, 74 (1965); J. C. D. BRAND AND J. L. HARDWICK, *Chem. Phys. Lett.* **21**, 458 (1973).
6. (a) K. ABE, *J. Mol. Spectrosc.* **48**, 395 (1973). (b) K. ABE, F. MEYERS, T. K. MCCUBBIN AND S. R. POLO, *J. Mol. Spectrosc.* **38**, 552 (1971); **50**, 413 (1974).
7. J. C. D. BRAND, J. L. HARDWICK, R. J. PIRKLE, AND C. J. SELISKAR, *Can. J. Phys.* **51**, 2184 (1973).
8. R. SOLARZ AND D. H. LEVY, *J. Chem. Phys.* **58**, 4026 (1973); R. SOLARZ, D. H. LEVY, K. ABE, AND R. F. CURL, *J. Chem. Phys.* **60**, 1158 (1974).
9. T. TANAKA, A. D. ENGLISH, R. W. FIELD, D. A. JENNINGS, AND D. O. HARRIS, *J. Chem. Phys.* **59**, 5217 (1973).
10. W. DEMTRÖDER, F. PAECH, AND R. SCHMIEDL, *Chem. Phys. Lett.* **26**, 381 (1974).
11. G. R. BIRD AND M. J. MARSDEN, *J. Mol. Spectrosc.* **50**, 403 (1974).
12. C. G. STEVENS, M. W. SWAGEL, R. WALLACE, AND R. N. ZARE, *Chem. Phys. Lett.* **18**, 465 (1973).
13. F. S. TOMPKINS AND M. FRED, *Appl. Opt.* **2**, 715 (1963).
14. A. GIACCHETTI, R. W. STANLEY, AND R. ZALUBIS, *J. Opt. Soc. Am.* **60**, 474 (1970).
15. G. HERZBERG, "Molecular Spectra and Molecular Structure," Vol. 3, Van Nostrand, Princeton, N. J., 1966.
16. S. C. HURLOCK, K. NARAHARI RAO, L. A. WELLER, AND P. K. L. YIN, *J. Mol. Spectrosc.* **48**, 372 (1973).
17. G. R. BIRD, J. C. BAIRD, A. W. JACHE, J. A. HODGESON, R. F. CURL, JR., A. C. KUNKLE, J. W. BRANSFORD, J. RASTRUP-ANDERSEN, AND J. ROSENTHAL, *J. Chem. Phys.* **40**, 3378 (1964); R. M. LEES, R. F. CURL, JR., AND J. G. BAKER, *J. Chem. Phys.* **45**, 2037 (1966).

18. J. T. HOUGEN, *J. Chem. Phys.* **39**, 358 (1963).
19. W. T. RAYNES, *J. Chem. Phys.* **41**, 3020 (1964).
20. C. C. LIN, *Phys. Rev.* **116**, 903 (1959).
21. T. TANAKA, R. W. FIELD, AND D. O. HARRIS, *J. Chem. Phys.*, in press.
22. A. D. WALSH, *J. Chem. Soc.*, 2266 (1953).
23. T. TANAKA, R. W. FIELD, AND D. O. HARRIS, *J. Mol. Spectrosc.* **56**, 188–199 (1975).
24. G. R. BIRD, *J. Chem. Phys.* **25**, 1040 (1956).
25. G. D. GILLESPIE, A. U. KHAN, R. P. HOSTENY, A. C. WAHL, AND M. KRAUSS, 29th Symposium on Molecular Structure and Spectroscopy, Columbus, Ohio, June 10–14, 1974, Book of Abstracts, FB6.